ELSEVIER

Chemical Engineering and Processing 41 (2002) 35–47

Chemical Engineering and Processing

www.elsevier.com/locate/cep

Simulation of the transient and steady state behaviour of a bubble column slurry reactor for Fischer–Tropsch synthesis

J.W.A. de Swart, R. Krishna *

Department of Chemical Engineering, University of Amsterdam, Nieuwe Achtergracht 166, 1018 WV Amsterdam, The Netherlands

Received 02 October 2000; received in revised form 05 December 2000; accepted 05 December 2000

Abstract

This paper develops a model to simulate the dynamic and steady-state behaviour of a commercial scale (diameter 7.5 m and dispersion height 30 m) Fischer–Tropsch bubble column slurry reactor operating in the churn-turbulent regime. A distinction is made between 'large' and 'small' bubble classes and the axial dispersion model is used to simulate their mixing behaviour and also of the liquid and catalyst particle phases.

The results of the dynamic simulations indicate that no thermal runaways are to be expected and that steady-state is achieved within about 7 min from start-up. Analysis of the steady-state behaviour shows that the hydrogen conversion in the reactor is mainly dictated by the 'large' bubbles, which account for a major fraction of the gas throughput.

Comparison of the commercial scale reactor performance with that of a smaller scale demonstration unit (of diameter 1 m and dispersion height 30 m) shows that due to significantly improved staging in the liquid phase, higher conversions are achieved in the demonstration unit. Furthermore, steep temperature gradients are to be expected in the demonstration unit, while these are absent in a reactor of commercial scale. The study underlines the need for accurate information on the liquid phase backmixing for scale up purposes.

Keywords: Steady state behaviour; Fischer–Tropsch synthesis; Bubble column slurry reactor

1. Introduction

It is expected that the demand for gasoil and kerosene (middle distillates) will grow in the near future, especially in the Asian region. Middle distillates can be distilled directly from crude oil, but can also be produced by converting coal or natural gas using the Fischer–Tropsch reaction. An advantage of using natural gas is that it is relatively abundant and can be converted into excellent quality (clean) middle distillates. From an economic point of view, potential processes need to be operated on a large scale [1–6]. Besides this, most of the large natural gas reserves are located in remote areas. These considerations make development and scale-up of potential processes both a difficult and challenging task. Shell [1] and Sasol [2,3] are currently the only companies having a Fischer–Tropsch middle distillates process in commercial operation. Several other major enterprises such as Exxon [4] are currently developing improved processes for conversion of natural gas to liquid products.

One of the most important subjects in the development of the Fischer–Tropsch process is the selection, design and scale-up of the reactor for the heavy paraffin synthesis. The Fischer–Tropsch reaction can be carried out in different reactor types. Published studies indicate that application of slurry technology is the most economical option [2,5–7]. In the past years numerous studies have been devoted to simulation of the Fischer–Tropsch slurry reactor [8–14]. Most of the literature models and studies were focused on operation at relative low superficial gas velocities (below about 0.10 m/s). Furthermore, operation at low gas velocities, in homogeneous bubbly flow regime, was considered to be the preferred option for a commercial Fischer–Tropsch slurry reactor. However, De Swart et al. [7] showed that for commercial operation higher gas velocities in the

* Corresponding author. Tel.: +31-20-5257007; fax: +31-20-5255604.

E-mail address: krishna@its.chem.uva.nl (R. Krishna).

0255-2701/02/$ - see front matter
PII: S0255-2701(00)00159-8

churn-turbulent flow regime is much more attractive from a commercial view point. Therefore, it is essential to model the churn-turbulent flow regime. This requires taking proper account of the presence of 'large' and 'small' bubbles as discussed by Krishna and co-workers [15–30]. Furthermore, none of the previous studies investigated the dynamic behaviour of the Fischer–Tropsch slurry reactor. There is no existing model in the literature which takes proper account of the hydrodynamics in the churn-turbulent flow regime and further accounts for the dynamic behaviour of the reactor.

In this study a dynamic model for simulation of a commercial Fischer–Tropsch slurry reactor is developed. This model is applicable to the churn-turbulent regime of operation and incorporates important and new information on the gas holdup and mass transfer [19–24] in slurry bubble columns. The axial dispersion model is adopted to properly describe the flow patterns of the 'large' bubbles, 'small' bubbles, liquid phase and catalyst particles. With the computer model developed, simulations are performed to identify the dynamic and steady state behaviour of a Fischer–Tropsch slurry reactor of commercial size.

2. Reaction scheme

The Fischer–Tropsch reaction catalytically converts synthesis gas into hydrocarbons. The reaction involves a chain-growth mechanism which implies that it is theoretically impossible to produce a product of single carbon number. The carbon number distribution of the products usually shows a Anderson–Flory–Schulz distribution which is characterized by the probability for chain growth α [1,5]. The parameter α depends on the catalyst formulation and operating conditions as reaction pressure and temperature. The synthesis of hydrocarbons from syngas catalyzed by iron, ruthenium or cobalt catalysts is known to lead to products which are highly linear in nature. In this study a cobalt catalyst is chosen and the reaction rate is assumed to be first order in hydrogen. The kinetics of the reaction are obtained from Post et al. [31] and α is assumed to be equal to 0.92. In the design and optimization procedure the following reaction is considered:

$$CO + 2H_2 \rightarrow -CH_2- + H_2O \quad (1)$$

so the usage ratio of hydrogen and carbon monoxide UR equals 2. The inlet ratio of hydrogen and carbon monoxide in the syngas mixture IR is taken equal to the usage ratio. The rate of the water gas shift reaction

$$CO + H_2O \rightarrow CO_2 + H_2 \quad (2)$$

is assumed to be negligible.

3. Hydrodynamic picture

This study focuses on a commercial Fischer–Tropsch slurry reactor operating in the churn-turbulent flow regime. For a slurry bubble column operating in the churn-turbulent flow regime the gas phase can be split up in a 'large' bubble population and a 'small' bubble population, as discussed in our earlier publications [19–24]. Coalescence of 'small' bubbles yields 'large' bubbles and bubble clusters which have a high rise velocity, typically in the range of 1–2 m/s. Due to the high rise velocity of these 'large' bubbles, high gas throughputs can be achieved, which is desirable from a commercial point of view due to economy of scale. It can be established visually that the 'large' bubbles traverse the column virtually in plug flow, often in a zig–zag, snake-like, fashion. They 'churn' up the liquid phase and cause intense mixing. In the churn-turbulent flow regime, we also have 'small' bubbles co-existing with the 'large' bubbles. These 'small' bubbles are 'entrained' in the liquid phase and have the backmixing characteristics of the liquid. A convenient way to model a reactor operating in the churn-turbulent flow regime is to extend the two-phase ('dilute' and 'dense' phases) model proposed by Van Deemter [32] for gas solid fluidized beds. This extension was suggested by Krishna [17–21]. Essentially, the key to the generalized two-phase model is to properly identify the 'dilute' and 'dense' phases. The superficial gas velocity U_{sg} is split in two parts: a part of the gas rises through the column in the form of 'small' bubbles at a superficial gas velocity U_{df}; the remainder rises through the column in the form of 'large' bubbles at a superficial gas velocity ($U_{sg} - U_{df}$). The dilute phase is to be identified with the 'large' bubble fraction and the dense phase with the 'small' bubble fraction together with liquid containing the catalyst particles in suspension. The 'dilute' phase can be considered to be virtually in plug flow, while the 'dense' phase is highly backmixed.

The Fischer–Tropsch slurry reactor is modeled according to the picture shown in Fig. 1. The gas phase enters the reactor at the bottom and is distributed into the suspension of liquid products and catalyst by a distributor plate. The reactor is operated in a co-current mode with respect to gas and slurry: fresh oil slurry enters the reactor at the bottom. As concluded by Mills et al. [12], countercurrent operation does not offer advantages; catalyst settling tendencies are increased which leads to inferior reactor performance during countercurrent operation. The reaction heat is removed from the reactor by means of cooling tubes inserted in the reactor.

In this study separate mass balances (based on the axial dispersion model) are set up for the 'large' bubbles, 'small' bubbles, liquid phase and the catalyst. The energy balance is set up for the liquid phase to calculate

the reactor temperature. The catalyst concentration profile over the reactor height is predicted using the sedimentation–dispersion model, as proposed by Kato et al. [33].

4. Model equations

As mentioned in the introduction, the axial dispersion model is adopted to describe the flow characteristics of the Fischer–Tropsch slurry reactor. In recent years there has been some discussion on the suitability of the axial dispersion model to properly account for the flow and mixing characteristics of the phases in a slurry bubble column [12,34,35]. The discussed issues are the suitability of the axial dispersion coefficient as single parameter to account for the axial and radial flow of the slurry phase and the ability of the axial dispersion model to account for different bubble classes. We believe that it is essential to introduce different balance equations into the model for the 'large' and 'small' bubble classes. This in order to correctly account for the residence time distribution of the gas phase in the reactor. Proper description of the mixing characteristics of the slurry phase by the axial dispersion coefficient as a single parameter is indeed questionable, but until more sophisticated hydrodynamic models become available the axial dispersion model is still the most convenient one.

The model proposed by Mills et al. [12] is used as a basis but extended to include the presence of two bubble classes, 'large' and 'small', characteristic of the churn-turbulent regime of operation. The developed model incorporates the following assumptions:

- the resistance for mass transfer between the gas and liquid phase is located in the liquid phase;
- the gas phase is in thermal equilibrium with the liquid phase;
- the catalyst is in thermal equilibrium with the liquid phase and intra particle temperature gradients do not exist;
- the superficial gas velocity at the reactor inlet and the superficial velocity of the slurry do not change during the operation;
- in the fresh oil slurry entering the reactor dissolved hydrogen is absent;
- the variation in gas flow rate in the reactor can be taken into account by application of a gas phase contraction factor *ALPHA*, defined as in Levenspiel [36]:

$$\mathrm{ALPHA} = \frac{V_g(X_{CO+H_2}=1) - V_g(X_{CO+H_2}=0)}{V_g(X_{CO+H_2}=0)} \tag{3}$$

The synthesis gas conversion X_{CO+H_2} can be expressed in terms of the inlet ratio *IR* and usage ratio *UR* of hydrogen and carbon monoxide:

$$X_{CO+H_2} = \frac{1+UR}{1+IR} X_{H_2} \tag{4}$$

The hydrogen conversion is defined as:

$$X_{H_2} = \frac{U_{sg0}\dfrac{C_{H_2,g0}}{C_g} - U_{sg}\dfrac{C_{H_2,g}}{C_g}}{U_{sg0}\dfrac{C_{H_2,g0}}{C_g}} \tag{5}$$

For the superficial gas velocity the following relation holds:

$$U_{sg} = U_{sg0}(1 + \mathrm{ALPHA}\ \ X_{CO+H_2}) \tag{6}$$

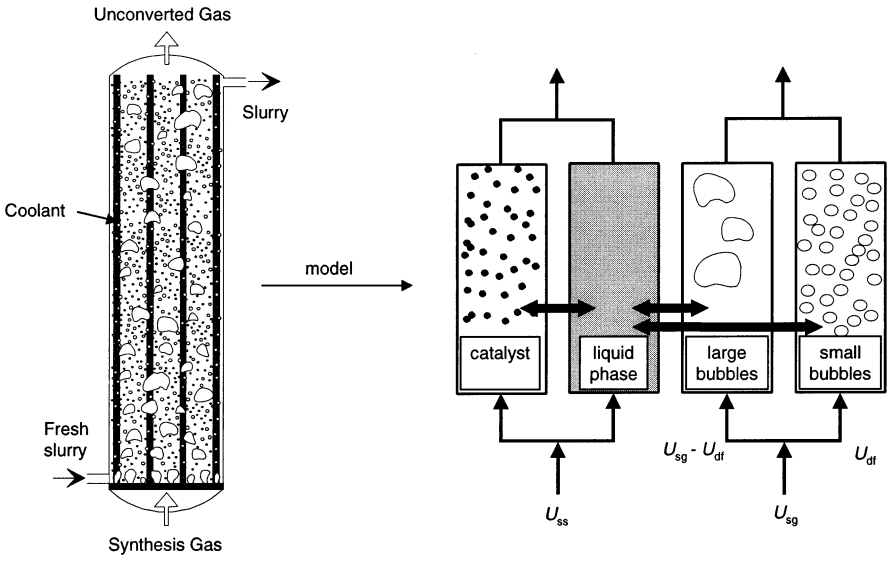

Fig. 1. Schematic representation of the reactor model for a commercial Fischer–Tropsch slurry reactor operating in the churn turbulent flow regime.

For equal inlet and usage ratio, substitution of Eqs. (4) and (5) in Eq. (6) yields the following relation for the variable superficial gas velocity:

$$U_{sg} = U_{sg0}\left(1 + \mathrm{ALPHA}\left(\frac{U_{sg0}\frac{C_{H_2,g0}}{C_g} - U_{sg}\frac{C_{H_2,g}}{C_g}}{U_{sg0}\frac{C_{H_2,g0}}{C_g}}\right)\right) \quad (7)$$

- the superficial gas velocity through the 'small' bubbles is constant over the reactor height;
- the effectiveness factor approaches unity; this assumption is justified because the mean particle diameter is 50 μm [31];
- the Fischer–Tropsch reaction is first order in hydrogen and hydrogen is considered to be the limiting component in the reaction.

Since hydrogen is considered the limiting component the balance equations are set up for hydrogen. The gas phase hydrogen concentrations in the 'large' and 'small' bubbles are made dimensionless by normalisation with respect to the hydrogen concentration at the inlet of the reactor; $y_{large} = C_{H_2,g,large}/C_{H_2,g0}$; $y_{small} = C_{H_2,g,small}/C_{H_2,g0}$.The liquid phase concentration of hydrogen is made dimensionless by normalization with respect to the hydrogen concentration in equilibrium with the gas phase concentration at the reactor inlet; $x = mC_{H_2,L}/C_{H_2,g0}$.The dimensionless temperature is obtained by normalization with respect to the coolant temperature, $\theta = T/T_c$. The dimensionless distance along the height of the reactor is $\xi = h/H$. A dimensionless time coordinate is defined as $\tau = (tU_{g0}/H)$. The various dimensionless groups used in the model are summarized in Table 1.

In analogy with Mills et al. [12], the mass and energy balances are applied over a differential element of the reactor. The resulting dimensionless equations are presented below.

The hydrogen balance for the 'large' bubbles:

$$\varepsilon_b\frac{\partial y_{large}}{\partial\tau} = \frac{\varepsilon_b}{Pe_{g,large}}\frac{\partial^2 y_{large}}{\partial\xi^2} - \frac{1+\mathrm{ALPHA}}{(1+\mathrm{ALPHA}\ y_{large})^2}\frac{(U_{sg}-U_{df})_0}{U_{g0}}\frac{\partial y_{large}}{\partial\xi} - \mathrm{St}_{g,large}(y_{large}-x) \quad (8)$$

The hydrogen balance for the 'small' bubbles:

$$\varepsilon_{small}\frac{\partial y_{small}}{\partial\tau} = \frac{\varepsilon_{small}}{Pe_{g,small}}\frac{\partial^2 y_{small}}{\partial\xi^2} - \frac{U_{df}}{U_{g0}}\frac{\partial y_{small}}{\partial\xi} - \mathrm{St}_{g,small}(y_{small}-x) \quad (9)$$

The hydrogen balance in the liquid phase:

$$\varepsilon_L\frac{\partial x}{\partial\tau} = \frac{\varepsilon_L}{Pe_L}\frac{\partial^2 x}{\partial\xi^2} - \frac{U_{ss}}{U_{g0}}\frac{\partial x}{\partial\xi} + \mathrm{St}_{L,\,large}(y_{large}-x) + \mathrm{St}_{L,\,small}(y_{small}-x) - C_s\,\mathrm{Da}\,\exp\left(-\frac{\gamma}{\theta}\right)x \quad (10)$$

Table 1
Dimensionless numbers appearing in the reactor model

Dimensionless number	Variable	Definition
Time	τ	$t\ U_{g0}/H$
Axial position	ξ	h/H
Slurry temperature	θ	T/T_c
Gas concentration large bubbles	y_{large}	$C_{H_2,g,large}/C_{H_2,g0}$
Gas concentration small bubbles	y_{small}	$C_{H_2,g,small}/C_{H_2,g0}$
Liquid concentration	x	$C_{H_2,L}m/C_{H_2,g0}$
Heat of reaction	Be	$-\Delta H_R C_{H_2,g0}/\rho_s\ C_{ps}\ m\ T_c$
Damköhler number first order reaction	Da	$k_{H_2}\varepsilon_L H/U_{g0}$
Bodenstein number catalyst	Bo_c	$Pe_c[U_{ct}/U_{g0} - U_{ss}/(U_{g0}(1-\varepsilon_g))]$
Peclet number 'large' bubbles	$Pe_{g,large}$	$U_{g0}H/E_{g,large}$
Peclet number 'small' bubbles	$Pe_{g,small}$	$U_{g0}H/E_{g,small}$
Peclet number liquid phase	Pe_L	$U_{g0}H/E_L$
Peclet number heat transfer	Pe_H	$\rho_s C_{ps} U_{g0} H/\lambda_{ax}$
Peclet number catalyst	Pe_c	$U_{g0}H/E_c$
Stanton number gas–liquid, gas side, 'large' bubbles	$St_{g,large}$	$k_{L,H_2,large}a_{large}H/mU_{g0}$
Stanton number gas-liquid, gas side, 'small' bubbles	$St_{g,small}$	$k_{L,H_2,small}\ a_{small}H/mU_{g0}$
Stanton number gas-liquid, liquid side, 'large' bubbles	$St_{L,large}$	$k_{L,H_2,large}a_{large}H/U_{g0}$
Stanton number gas-liquid, liquid side, 'small' bubbles	$St_{L,small}$	$k_{L,H_2,small}a_{small}H/U_{g0}$
Stanton number heat transfer	St_H	$\alpha_{eff}a_w H/\rho_s C_{ps} U_{g0}$
Conversion of hydrogen in the gas phase	X_{H_2}	see eq. (5)
Arrhenius number	γ	$E_a/(RT_c)$

Mass balance for the catalyst particles in the slurry phase

$$C_s(\xi) = \overline{C_s}\frac{\mathrm{Bo_c}\exp(-\mathrm{Bo_c}\xi)}{1-\exp(-\mathrm{Bo_c})} \quad (11)$$

Energy balance for the slurry phase. The time variation of the temperature is determined by (a) dispersion, (b) convection, (c) reaction enthalpy and (d) heat removal through the tubes:

$$\varepsilon_L\frac{\partial\theta}{\partial\tau} = \frac{\varepsilon_L}{Pe_H}\frac{\partial^2\theta}{\partial\xi^2} - \frac{U_{ss}}{U_{sg0}}\frac{\partial\theta}{\partial\xi} + C_s\ Be\ \mathrm{Da}\exp\left(\frac{\gamma}{\theta}\right)x - \mathrm{St_H}(\theta-1) \quad (12)$$

Initial conditions for $0 \leqslant \xi \leqslant 1$:

$$\text{at } \tau = 0,\ y_{large} = y_{small} = x = 0 \quad (13)$$

$$C_s = C_{s0}(\xi) \quad (14)$$

$$T = T_w = T_c \quad (15)$$

Boundary conditions:

$$\text{at } \xi = 0\ y_{large} = 1 \quad (16)$$

$$\varepsilon_{small}\frac{\partial y_{small}}{\partial \xi} = Pe_{g,small}(y_{small}-1) \quad (17)$$

$$\varepsilon_L\frac{\partial x}{\partial \xi} = Pe_L\frac{U_{ss}}{U_{g0}}x \quad (18)$$

$$\varepsilon_L\frac{\partial \theta}{\partial \xi} = Pe_H\frac{U_{ss}}{U_{g0}}(\theta-1) \quad (19)$$

$$\text{at } \xi = 1 \ \frac{\partial y_{small}}{\partial \xi} = 0 \quad (20)$$

$$\frac{\partial y_{large}}{\partial \xi} = 0 \quad (21)$$

$$\frac{\partial x}{\partial \xi} = 0 \quad (22)$$

$$\frac{\partial \theta}{\partial \xi} = 0 \quad (23)$$

Eqs. (8)–(12) together with the initial conditions (13)–(15) and the boundary conditions (16)–(23) form the complete reactor model.

5. Parameter values

The following physical properties were used: $\eta_L = 6.0\times10^{-4}$ Pa s [31]; $\sigma = 0.019$ Pa m [37]; $\rho_L = 680$ kg m^{-3} [37]; $\lambda_L = 0.113$ W m^{-1} K^{-1}; $C_{pL} = 424$ J mol^{-1} K^{-1}; $M_L = 0.283$ kg mol^{-1}; $D_{H_2} = 5.54\times10^{-8}$ m^2 s^{-1} [38]; $m = 5.095$ [39]; $d_p = 50\times10^{-6}$ m; $\rho_p = 1200$ kg m^{-3}; $C_{pC} = 993$ J kg^{-1} K^{-1}; $\lambda_p = 1.7$ W m^{-1} K^{-1}; $\eta_G = 2.0\times10^{-5}$ Pa s; $\lambda_G = 0.186$ W m^{-1} K^{-1}; The physical properties of the suspension are summarized in Table 2.

The kinetic parameters are obtained from Post et al. [31] and are summarized in Table 3. The reactor operates at a pressure of 40 bar. In all the simulations the average reactor temperature equals 513 K. Cooling of the reactor is established by 0.05 m diameter cooling tubes. In order to keep the mean temperature at 513 K, the area available for heat transfer a_w is varied between 5 and 19 m^2 (m^3 reactor)$^{-1}$, depending on the operating conditions. A constant coolant temperature T_c of 501 K is used in the simulations. The contraction factor ALPHA is assumed to be equal to -0.5 [9]. All simulations are performed with a 7.5 m diameter reactor having a dispersion height $H = 30$ m. The catalyst volume fraction in the gas free slurry C_s equals 0.25 in all simulations. The reactor is operated in a co-current mode with respect to gas and slurry, the superficial velocity of the slurry U_{ss} equals 0.01 m/s in all simulations. The settling velocity of the catalyst particles in a swarm U_{ct} is calculated according to Mills et al. [12]. In the hydrodynamic relations where the superficial gas velocity is involved, the value of U_{sg} at the inlet of the reactor is taken.

Table 2
Physical properties of the slurry

Slurry properties	Definition	Dimensions
Catalyst weight fraction in suspension	$W_c = \frac{C_s\rho_p}{C_s(\rho_p-\rho_L)+\rho_L}$	dimensionless
Suspension density	$\rho_s = C_s\rho_p+(1-C_s)\rho_L$	kg m^{-3}
Suspension specific heat	$C_{ps} = W_cC_{pC}+(1-W_c)C_{pL}$	J kg^{-1} K^{-1}
Suspension viscosity	$\eta_s = \eta_L(1+4.5C_s)$	Pa s
Suspension heat conductivity	$\lambda_s = \lambda_L\frac{2\lambda_L+\lambda_p-2C_s(\lambda_L-\lambda_p)}{2\lambda_L+\lambda_p+C_s(\lambda_L-\lambda_p)}$	W m^{-1} K^{-1}
Suspension effective axial heat conductivity	$\lambda_{ax} = E_LC_{ps}\rho_s$	W m^{-1} K^{-1}

The gas holdup at which transition from the homogeneous to the churn turbulent flow regime occurs (ε_{trans}) depends on the gas density ρ_g, liquid viscosity η_L, surface tension σ and the catalyst concentration C_s. For design purposes ε_{trans} can be estimated using the relation proposed by De Swart [30]:

$$\varepsilon_{trans} = 2.16\exp(-13.1\ \rho_g^{-0.10}\eta_L^{0.16}\sigma^{0.11})\exp(-5.86\ C_s) \quad (24)$$

The corresponding superficial gas velocity U_{trans} at regime transition is found from:

$$U_{trans} = V_{small}\varepsilon_{trans} \quad (25)$$

where V_{small} is the rise velocity of the 'small' bubbles. An estimation of V_{small} can be obtained from the relation proposed by Wilkinson [40]:

$$V_{small} = 2.25\frac{\sigma}{\eta_L}\left(\frac{\sigma^3\rho_L}{g\eta_L^4}\right)^{-0.273}\left(\frac{\rho_L}{\rho_g}\right)^{0.03} \quad (26)$$

For churn turbulent operation the superficial gas velocity and gas holdup of the small bubbles are assumed to be equal to their values at the regime transi-

Table 3
Reaction rate parameters

Reaction parameters	Variable	Dimensions
Activation energy	$E_a = 1.181\times10^5$	J mol^{-1}
Pre-exponential factor	$A = 5.202\times10^{10}$	m^3 (m^3 catalyst)$^{-1}$ s^{-1}
First order reaction rate constant for hydrogen	$k_{H2} = A\ m\exp(-E_a/RT)$	m^3 (m^3 catalyst)$^{-1}$ s^{-1}
Heat of reaction	$-\Delta H_R = 165\,000$J (mole syngas)$^{-1}$	

$$\varepsilon_{\text{small}}\frac{\partial y_{\text{small}}}{\partial \xi} = \text{Pe}_{\text{g,small}}(y_{\text{small}} - 1) \quad (17)$$

tion point: $\varepsilon_{\text{small}} = \varepsilon_{\text{trans}}$ and $U_{\text{df}} = U_{\text{trans}}$. The diameter of the 'small' bubbles is estimated from the relation of Wilkinson [40]:

$$d_{\text{s}} = 3g^{-0.44}\sigma^{0.34}\eta_{\text{L}}^{0.22}\rho_{\text{L}}^{-0.45}\rho_{\text{g}}^{-0.11}U_{\text{sg}}^{-0.02} \quad (27)$$

The effective interfacial area for mass transfer between the gas and liquid phase for the 'small' bubbles is now given by the relation:

$$a_{\text{small}} = \frac{6\varepsilon_{\text{small}}}{d_{\text{s}}} \quad (28)$$

The value of the mass transfer coefficient $k_{\text{L,H}_2\text{,small}}$ for the 'small' bubbles is predicted using the relation of Calderbank and Moo-Young [41] for rigid spherical bubbles.

The gas holdup of the 'large' bubbles ε_{b} depends on the scale of operation but is independent of slurry concentration, liquid properties [20–24] and of the system pressure [16]. The large bubble holdup is predicted using the model of Ellenberger and Krishna [18]. The mass transfer coefficient of the large bubbles $k_{\text{L,H}_2\text{,large}}$ is predicted using the relation proposed by Calderbank and Moo-Young [41] for bubbles not behaving as rigid spheres. The interfacial area for mass transfer of the large bubbles a_{large} is estimated using the relation proposed by Vermeer and Krishna [15]:

$$\frac{k_{\text{L,ref,large}}\, a_{\text{large}}}{\varepsilon_{\text{b}}} = 0.5 \quad \text{s}^{-1} \quad (29)$$

which is corrected for the mass transfer coefficient of hydrogen under the reaction conditions by the factor $k_{\text{L,H}_2\text{,large}}/k_{\text{L,ref,large}}$. The 'large' bubbles traverse the column virtually in plug flow and therefore the Peclet number of the large bubbles ($\text{Pe}_{\text{g, large}}$) is assigned a large value equal to 100. Due to their high rise velocities, the 'large' bubbles induce circulation patterns in the liquid phase. The 'small' bubbles are entrained in the liquid phase and the axial dispersion coefficient of the 'small' bubbles is assumed to be equal to the axial dispersion coefficient of the liquid phase ($E_{\text{g,small}} = E_{\text{L}}$); this assumption has been validated using CFD simulations [29]. The axial dispersion coefficient of the liquid phase is calculated using the relation proposed by Deckwer et al. [9]:

$$E_{\text{L}} = 0.768\ U_{\text{g0}}^{0.32}\ D_T^{1.34} \quad (30)$$

We will return to this relation at a later stage. The axial dispersion coefficient of the catalyst E_{c} is calculated according to Mills et al. [12].

The overall heat transfer coefficient α_{eff} is estimated using the relation proposed by Deckwer et al. [9], developed primarily for the homogeneous flow regime:

$$\alpha_{\text{eff}} = 0.1\ (\rho_{\text{s}}C_{\text{ps}}U_{\text{sg}})\left(\frac{U_{\text{sg}}^3\rho_{\text{s}}}{g\eta_{\text{s}}}\right)^{-\frac{1}{4}}\left(\frac{\rho_{\text{s}}C_{\text{ps}}}{\lambda_{\text{s}}}\right)^{-\frac{1}{2}} \quad (31)$$

For superficial gas velocities exceeding 0.10 m/s the heat transfer coefficient is to be calculated from Eq. (31) by taking U_{sg} equal to 0.10 m/s [9].

6. Numerical solution procedure

The complete reactor model is defined by the four partial differential Eqs. (8)–(12), together with the accompanying initial and boundary conditions. This set of partial differential equations is solved numerically using the Method of Lines (MOL), as proposed by Schiesser [42]. The method of lines discretizes a set of partial differential equations using a finite difference scheme to obtain a set of ordinary differential equations (ODE's). This set of ODE's is then solved simultaneously.

The reactor is discretized in $N = 60$ points. This results in $4 \times N = 240$ ordinary differential equations. The DSS/2 software package (Fortran 77 code from Silebi and Schiesser [43]) was used to discretize the reactor. The following DSS/2 subroutines were used:

- subroutine DSS002: one dimensional, three points centered approximations for first order approximations;
- subroutine DSS014: one dimensional, three points upwind approximations for first order derivatives.

The parabolic contribution $\partial^2 C/\partial h^2$ was calculated using the subroutine DSS002 twice. The hyperbolic contribution $U(\partial C/\partial h)$ was calculated using subroutine DSS014.

The ODE's are solved using the implicit LSODES integrator routine [44].

7. Start-up of the reactor

The start-up of a commercial Fischer–Tropsch slurry reactor is simulated using a reactor with a diameter of 7.5 m and a dispersion height of 30 m. At dimensionless times $\tau < 0$ an inert gas is considered to flow continuously through the reactor with a superficial gas velocity of 0.14 m/s. The hydrogen concentration in the 'small' bubbles (y_{small}), 'large' bubbles (y_{large}) and in the liquid phase (x) are equal to zero. The temperature in the reactor equals the temperature of the coolant ($\theta = 1$). At dimensionless time $\tau = 0$ a step change in the hydrogen and carbon monoxide concentration in the gas phase occurs to initiate the reaction and the feed gas composition is kept constant for $\tau > 0$.

Fig. 2 shows the dimensionless hydrogen concentration in the 'large' bubbles y_{large} as function of dimensionless time τ and reactor height ξ. At $\tau = 0$ there is no hydrogen present in the 'large' bubbles. For $\tau > 0$ the hydrogen concentration at the reactor inlet equals 1 and hydrogen starts to dissolve into the liquid phase

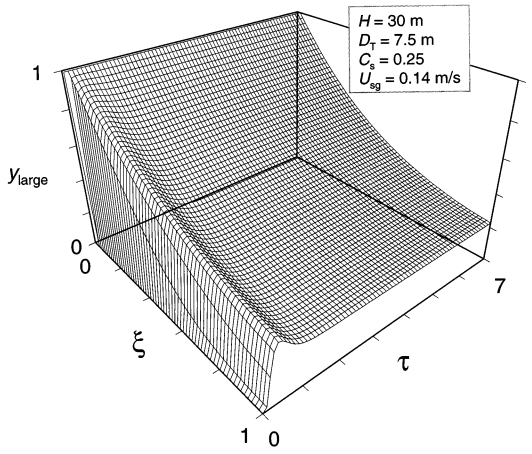

Fig. 2. Simulated start-up of a commercial Fischer–Tropsch slurry reactor with with a diameter D_T of 7.5 m and a dispersion height H of 30 m: Hydrogen concentration in the 'large' bubbles.

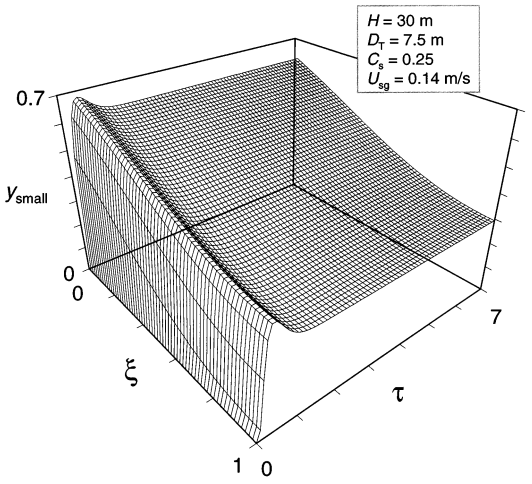

Fig. 4. Simulated start-up of a commercial Fischer–Tropsch slurry reactor with with a diameter D_T of 7.5 m and a dispersion height H of 30 m: Hydrogen concentration in the 'small' bubbles.

(see Fig. 3, the hydrogen concentration x in the liquid phase). As time τ increases, the liquid phase concentration increases and the hydrogen concentration profiles for the 'large' bubbles, 'small' bubbles (Fig. 4) and for the liquid phase begin to develop. As τ reaches the value of about two, corresponding to 7 min, the steady state profiles are reached. From Figs. 2–4 it can be seen that the hydrogen concentrations go through a maximum before reaching the steady state profiles. This can be explained after examination of Fig. 5, the dimensionless temperature θ as function of dimensionless time τ and reactor height ξ. Comparison of Fig. 5 with Figs. 2–4 reveals that the time interval before θ approaches a steady state value is *larger* than the times required for y_{large}, y_{small} and x to reach their stationary state values. In other words, *it takes more time for the reaction to heat up the reactor than it takes for the hydrogen to dissolve into the liquid phase and react*. Because of the slower response of the temperature, the reaction rate is still increasing due to the increasing temperature while the concentration profiles are at their maximum values. The increasing reaction rate increases the amount of hydrogen which is depleted in the liquid phase, so liquid phase hydrogen concentration begins to decrease until the temperature eventually reaches steady state.

From the simulations of the start-up of a commercial Fischer–Tropsch slurry reactor can be concluded that steady state is reached in about 7 min. Furthermore, no severe temperature peaks or run away trends are observed, which is an important conclusion for the very exothermic Fischer–Tropsch reaction.

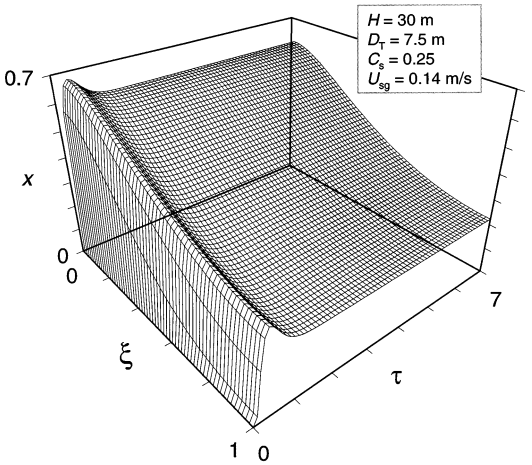

Fig. 3. Simulated start-up of a commercial Fischer–Tropsch slurry reactor with with a diameter D_T of 7.5 m and a dispersion height H of 30 m: Hydrogen concentration in the liquid phase.

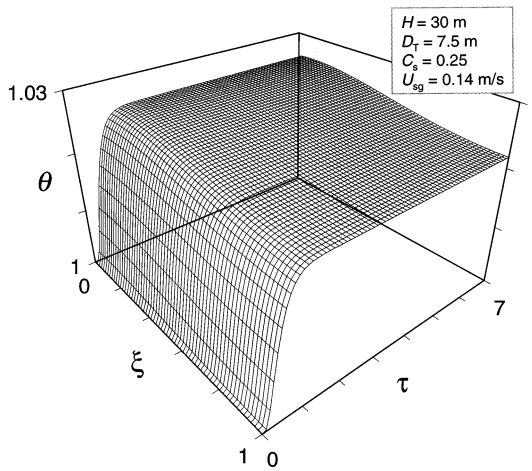

Fig. 5. Simulated start up of a commercial Fischer-Tropsch slurry reactor with with a diameter D_T of 7.5 m and a dispersion height H of 30 m: Reactor temperature.

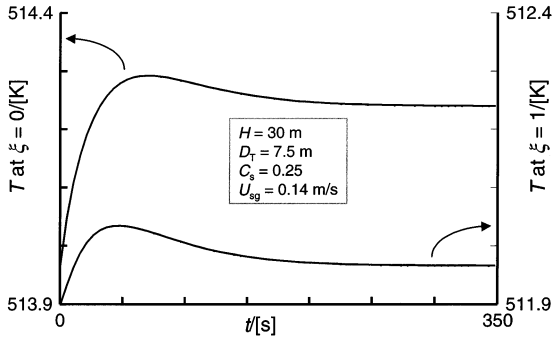

Fig. 6. Temperature response of a commercial Fischer–Tropsch slurry reactor with a diameter D_T of 7.5 m and a dispersion height H of 30 m to a step of 1 degree K in the coolant temperature.

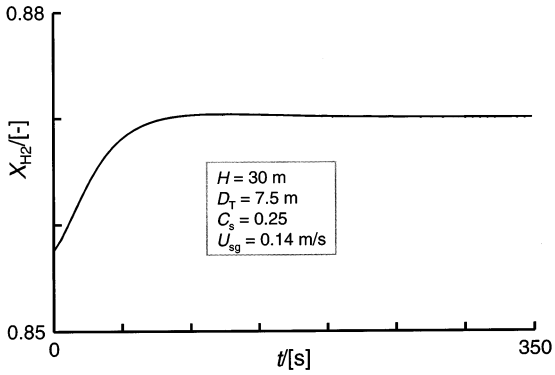

Fig. 7. Hydrogen conversion response of a commercial Fischer–Tropsch slurry reactor with a diameter D_T of 7.5 m and a dispersion height H of 30 m to a step of 1 degree K in the coolant temperature.

8. Stability to step disturbances

Because of the highly exothermic behaviour of the Fischer–Tropsch reaction, it is very important to confirm the thermal stability of the reactor. In order to establish this, the response of the reactor to step rise of 1 degree K in the coolant temperature is simulated. The reactor configuration is identical to the one simulated in the former section, $D_T = 7.5$ m, $H = 30$ m and $U_{sg} = 0.14$ m/s.

Fig. 6 shows the responses of the reactor temperature to the step change in the coolant temperature. The two lines in Fig. 6 represent the temperatures at the entrance of the reactor ($\xi = 0$) and at the outlet of the reactor ($\xi = 1$) for varying time. It can be seen that the temperature begins to rise after the step change is performed and reaches a new steady state in about 3 min. The resulting hydrogen conversion is shown in Fig. 7. The hydrogen conversion increases due to the increase in the temperature from about 0.86 to 0.87. No runaway tendencies are observed and it is established that the reactor operates under thermal stable conditions; this conclusion has been reached on the basis of several runs.

9. Steady state reactor behaviour

This section discusses results on the steady-state behaviour of a commercial Fischer–Tropsch slurry reactor. Simulations with the dynamic model are performed and the resulting steady state values of the output variables are presented. The influence of the superficial gas velocity and backmixing characteristics on the reactor performance are investigated.

Fig. 8 shows the hydrogen concentration profiles over the reactor height in the 'large' bubbles, 'small' bubbles and the liquid phase for a commercial Fischer–Tropsch slurry reactor with a diameter $D_T = 7.5$ m, dispersion height $H = 30$ m and operating with a superficial gas velocity $U_{sg} = 0.14$ m s^{-1}. It can be seen that the 'large' bubble concentration decreases from 1 at the inlet of the reactor to an equilibrium value with the liquid phase of about 0.25 at the outlet of the reactor. The 'small' bubbles suffer because of their backmixed character: they are almost in equilibrium with the liquid phase all over the reactor. Fig. 9a shows the temperature profile over the reactor. A rather flat profile exists due to the backmixed character of the liquid phase; the temperature difference is only 2 K between the inlet and the outlet of the reactor and no severe hot spots exist. The catalyst concentration profile is shown in Fig. 9b. It can be seen that the catalyst concentration is highest at the top of the reactor. This is due to the fact that the settling velocity of the particles in a swarm is lower than the superficial velocity of the liquid phase. The gradient of the catalyst over the reactor however is very small which implies that operational problems due to catalyst settling tendencies are not to be expected.

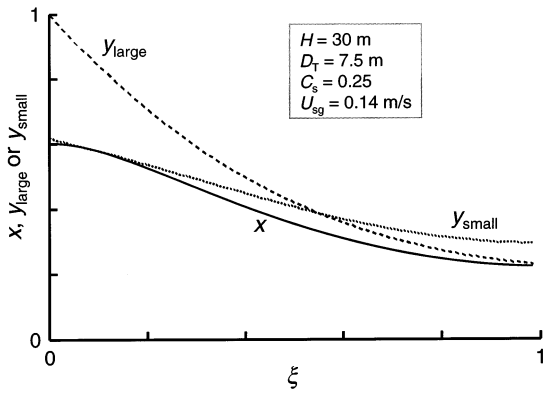

Fig. 8. Hydrogen concentration profiles in a commercial Fischer–Tropsch slurry reactor with a diameter D_T of 7.5 m and a dispersion height H of 30 m for hydrogen in the liquid phase, "large" bubbles and 'small' bubbles.

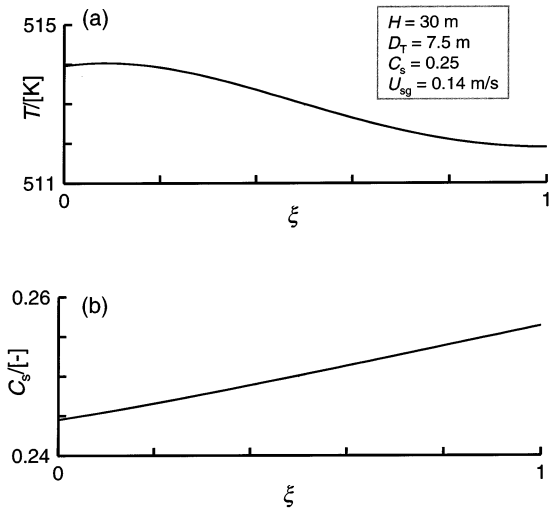

Fig. 9. Reactor profiles in a commercial Fischer–Tropsch slurry reactor with a diameter D_T of 7.5 m and a dispersion height H of 30 m for (a) the temperature and (b) the catalyst.

Simulations are performed for the same reactor configuration to identify the influence of the superficial gas velocity on the performance of the Fischer–Tropsch slurry reactor. The gas velocity U_{sg} is varied between 0.04 and 0.24 m/s, so operation well into the churn turbulent flow regime is considered (the superficial gas velocity at the regime transition point U_{trans} is estimated to be 0.01 m/s). Fig. 10 shows that the hydrogen conversion X_{H_2} decreases as the superficial gas velocity is increased. Also shown in Fig. 10 is a continuous line which represents the hydrogen conversion obtained on ignoring the mass transfer contribution of the 'small' bubble population ($k_{L,H_2,small} = 0$). It can be seen that the overall hydrogen conversion at superficial gas velocities above 0.10 m/s is largely determined by the conversion of the 'large' bubbles. Fig. 11 shows that the reactor throughput of the 'large' bubbles is also much larger than the throughput of the 'small'

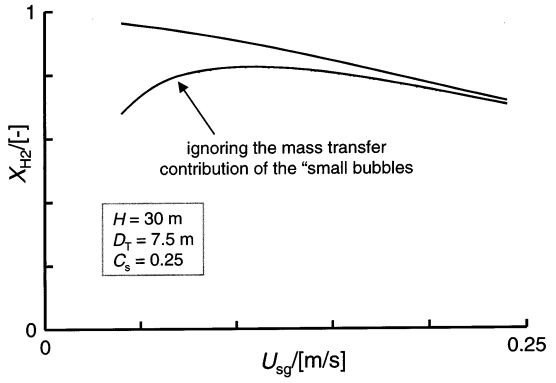

Fig. 10. Influence of the superficial gas velocity U_{sg} on the hydrogen overall and 'large' bubble hydrogen conversion in a commercial Fischer–Tropsch slurry reactor with a diameter D_T of 7.5 m and a dispersion height H of 30 m.

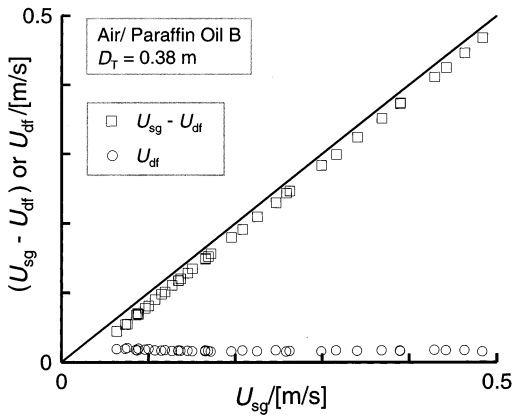

Fig. 11. Representation of $(U_{sg} - U_{df})$, representing the throughput of the 'large' bubbles, and U_{df}, representing the throughput of the 'small' bubbles for varying superficial gas velocities. Data taken from experiments reported in De Swart and Krishna (1996).

bubbles. So for the Fischer–Tropsch slurry reactor operating at superficial gas velocities above 0.10 m s^{-1} the reactor throughput and conversion are largely determined by the 'large' bubbles.

For the prediction of the axial dispersion coefficient of the liquid phase Eq. (30) of Deckwer et al. [9] is adopted. As the level of mixing of the liquid phase has a very strong influence on the predicted conversion in a Fischer–Tropsch slurry reactor (see for example Bukur [8]), accurate prediction of the axial dispersion coefficient for commercial scale reactors is of paramount importance. However, the highest diameter for which Eq. (30) has been verified is 3.20 m, but operation was limited to a superficial gas velocity of only 0.05 m/s [45]. Because their is much uncertainty in extrapolating Eq. (30) to commercial diameters for the Fischer–Tropsch slurry reactor (say 8 m), simulations are performed with the maximum diameter in the backmixing relation set at a value of 1 m. Fig. 12 shows the resulting hydrogen conversions for varying superficial gas velocities ($D_T = 7.5$ m and $H = 30$ m). Setting the value of

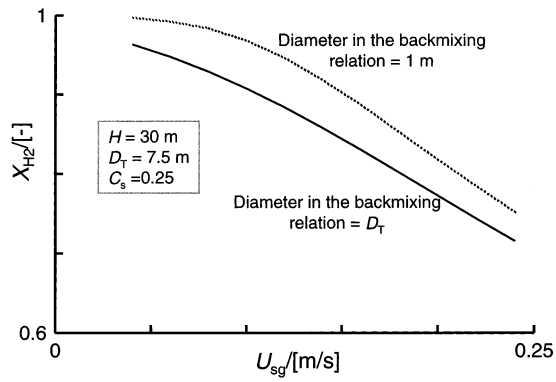

Fig. 12. Hydrogen conversion levels for different backmixing levels of the liquid phase in a commercial Fischer–Tropsch slurry reactor with a diameter D_T of 7.5 m and a dispersion height H of 30 m.

the diameter in the backmixing relation at a constant value of 1 m decreases the axial dispersion coefficient significantly and leads to increased plug flow character of the liquid phase. Increased plug flow character leads to higher conversions of hydrogen, as shown in Fig. 12. Increased plug flow character also changes the temperature profile over the reactor significantly, as shown in Fig. 13 for a superficial gas velocity of 0.14 m/s. The temperature gradient increases from 2 K to about 20 K and a small temperature peak near the inlet of the reactor is observed. From these simulations can be concluded that a key for a successful scale-up procedure for the Fischer–Tropsch slurry reactor is the amount of backmixing in the liquid phase. In the open literature many studies and correlations are presented, but validation of these correlations is limited to laboratory scale equipment. For the design of commercial Fischer–Tropsch slurry reactor it is desirable to validate the correlations for reactor diameters up to 8 m and superficial gas velocities up to 0.5 m/s.

10. Conclusions

The conclusions emerging from the computer model for a commercial Fischer–Tropsch slurry reactor operating in the churn-turbulent flow regime are summarized below:

- The start-up of the reactor is simulated and it can be concluded that steady state is reached in about 7 min. Furthermore, no severe temperature peaks or runaway trends are observed.
- For highly exothermic reactions as the Fischer–Tropsch reaction thermal stability of the reactor is of utmost importance. Simulations indicate that the Fischer–Tropsch slurry reactor simulated in this study operates under thermal stable conditions.

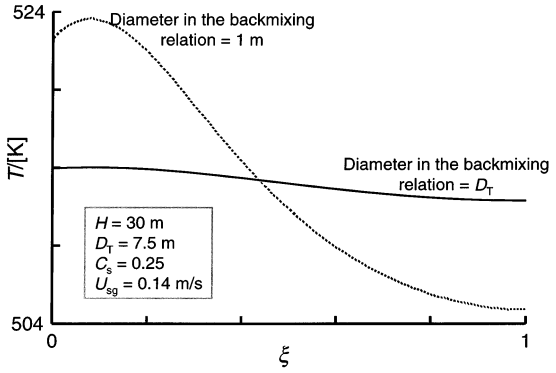

Fig. 13. Temperature profiles over the reactor for different backmixing levels of the liquid phase in a commercial Fischer–Tropsch slurry reactor with a diameter D_T of 7.5 m and a dispersion height H of 30 m.

- Because of reasons of isothermal operation catalyst settling tendencies are to be avoided. Operation with an upflow superficial velocity of the slurry U_{ss} of 0.01 m/s results in a rather flat catalyst profile over the reactor
- The level of backmixing in the liquid phase is an important parameter in predicting conversion levels and temperature profiles for commercial Fischer–Tropsch slurry reactors. Existing correlations are not tested in the open literature for the reactor diameters adopted for commercial operation (≈ 8 m). Furthermore, the correlations are tested in systems without cooling tubes. Both the influence of commercial diameters and cooling tubes on the backmixing are subjects which need further investigation.

Though this paper has considered the simulation of a commercial reactor, the developed model will also be vital for simulation of a pilot plant. Typically a pilot plant reactor will be 0.1–0.2 m in diameter. This means that the "dense" phase can be considered to be in plug flow. Our model will help translate pilot plant data to commercial units.

Appendix A. Nomenclature

a_{large}	gas–liquid specific interfacial area for the 'large' bubbles per unit expanded bed volume ($m^2\ m^{-3}$)
a_{small}	gas–liquid specific interfacial area for the 'small' per unit expanded bed volume ($m^2\ m^{-3}$)
a_w	cooling tube specific external surface area referred to the total reactor volume ($m^2\ m^{-3}$)
ALPHA	modified contraction factor (dimensionless)
C_g	gas phase concentration (mol m^{-3})
$C_{H_2,g0}$	concentration of hydrogen in the gas phase at the reactor inlet (mol m^{-3})
$C_{H_2,g,large}$	concentration of hydrogen in the 'large' bubbles (mol m^{-3})
$C_{H_2,g,small}$	Concentration of hydrogen in the 'small' bubbles (mol m^{-3})
$C_{H_2,L}$	Concentration of hydrogen in the liquid phase (mol m^{-3})
$C_{p,c}$	Heat capacity of the catalyst particles (J kg^{-1} K^{-1})
$C_{p,L}$	Heat capacity of the liquid (J kg^{-1} K^{-1})
$C_{p,s}$	Heat capacity of the liquid-solid suspension (J kg^{-1} K^{-1})

C_s	Solids volume fraction in gas free slurry (dimensionless)
$\bar{C}_s$	Mean solids volume fraction in gas free slurry in the reactor (dimensionless)
d_p	Particle diameter (m)
d_s	Diameter of 'small' bubbles (m)
d_t	tube diameter (m)
D	Liquid phase diffusivity ($m^2\ s^{-1}$)
D_T	Column diameter (m)
E_a	Activation energy ($J\ mol^{-1}$)
$E_{g,large}$	axial dispersion coefficient of the large bubbles ($m^2\ s^{-1}$)
$E_{g,small}$	axial dispersion coefficient of the small bubbles ($m^2\ s^{-1}$)
E_L	axial dispersion coefficient of the liquid phase ($m^2\ s^{-1}$)
E_c	axial dispersion coefficient of the catalyst particles ($m^2\ s^{-1}$)
$\boldsymbol{G}$	Acceleration due to gravity (9.81 m s^{-2})
H	Height above the gas distributor (m)
H	Height of expanded bed (m)
$-\Delta H_R$	heat of reaction for the overall conversion of synthesis gas to hydrocarbons ($J\ mol^{-1}$)
IR	Molar ratio of hydrogen to carbon monoxide at the reactor inlet (dimensionless)
k_{H_2}	first order reaction rate constant (s^{-1})
$k_{LH_2,small}$	Liquid phase mass transfer coefficient of species j at the 'small' bubble gas–liquid interface ($m\ s^{-1}$)
M	Distribution coefficient (dimensionless)
P	total pressure (Pa)
R	gas constant ($J\ mol^{-1}\ K^{-1}$)
STY	Space time yield (kg hydrocarbons $(m^3$ reactor$)^{-1}\ h^{-1}$)
T	time (s)
T	Temperature (K)
T_c	Cooling tube temperature (K)
UR	Usage ratio of hydrogen to carbon monoxide (dimensionless)
U_{ct}	Settling velocity of the catalyst particles in a swarm ($m\ s^{-1}$)
U_{df}	Superficial velocity of gas through the dense phase ($m\ s^{-1}$)
U_{sg}	Superficial gas velocity ($m\ s^{-1}$)
$(U_{sg}-U_{df})$	Superficial gas velocity through the dilute phase ($m\ s^{-1}$)
U_{ss}	Superficial slurry velocity ($m\ s^{-1}$)
U_{trans}	Superficial gas velocity at regime transition ($m\ s^{-1}$)
V_b	rise velocity of the large bubble population ($m\ s^{-1}$)
V_{small}	rise velocity of small bubble population ($m\ s^{-1}$)
W_s	Weight fraction of catalyst in gas free slurry (dimensionless)
X	Dimensionless hydrogen concentration in the liquid phase (dimensionless)
y_{large}	Dimensionless hydrogen concentration in the 'large' bubbles (dimensionless)
y_{small}	Dimensionless hydrogen concentration in the 'small' bubbles (dimensionless)
X_{H_2}	Conversion of hydrogen (dimensionless)

Greek letters

α_{eff}	Slurry to internal coil wall convective heat transfer coefficient ($W\ m^{-2}\ K^{-1}$)
γ	Arrhenius number (E_a/RT_c)
ε_g	total gas hold-up (dimensionless)
ε_b	gas hold-up of 'large' bubbles (dimensionless)
ε_L	Liquid holdup (dimensionless)
ε_{small}	hold-up of small bubbles ('dense' phase gas) (dimensionless)
ε_{trans}	gas hold-up at the regime transition point (dimensionless)
η_L	Liquid viscosity (Pa s)
η_s	Suspension viscosity (Pa s)
θ	Temperature of the liquid–solid suspension referred to the wall temperature, T/T_c (dimensionless)
λ_{ax}	effective axial heat conductivity of the liquid–solid suspension ($W\ m^{-1}\ K^{-1}$)
λ_c	heat conductivity of the catalyst particles ($W\ m^{-1}\ K^{-1}$)
λ_g	heat conductivity of the gas ($W\ m^{-1}\ K^{-1}$)
λ_L	heat conductivity of the liquid ($W\ m^{-1}\ K^{-1}$)
λ_s	heat conductivity of the liquid–solid suspension ($W\ m^{-1}\ K^{-1}$)
ξ	axial coordinate, h/H (dimensionless)
ρ_g	gas density ($kg\ m^{-3}$)
ρ_L	liquid density ($kg\ m^{-3}$)
ρ_p	particle density ($kg\ m^{-3}$)
ρ_s	suspension density ($kg\ m^{-3}$)
σ	surface tension of liquid phase (Pa m)

τ	dimensionless time coordinate (dimensionless)

References

[1] S.T. Sie, M.M.G. Senden, H.M.H. Van Wechem, Conversion of natural gas to transportation fuels via the Shell Middle Distillates process (SMDS), Catalysis Today 8 (1971) 371–394.

[2] B. Jager, R. Espinoza, Advances in low temperature Fischer–Tropsch synthesis, Catalysis Today 23 (1995) 17–28.

[3] B. Jager, Developments in Fischer–Tropsch technology, Studies in Surface Science and Catalysis 119 (1998) 25–34.

[4] B Eisenberg, R.A. Fiato, C.H. Mauldin, G.R. Say, S.L. Soled, Exxon's advanced gas-to-liquids technology, Studies in Surface Science and Catalysis 119 (1998) 943–948.

[5] S.T. Sie, R. Krishna, Fundamentals and selection of advanced Fischer–Tropsch reactors, Applied Catalysis A 186 (1999) 55–70.

[6] R. Krishna, S.T. Sie, Selection, design and scale-up Aspects of Fischer–Tropsch Reactors, Fuel Processing Tech. 64 (2000) 73–105.

[7] J.W.A. De Swart, R. Krishna, S.T. Sie, Selection, design and scale up of the Fischer–Tropsch slurry reactor, Studies in Surface Science and Catalysis 107 (1997) 213–218.

[8] D.B Bukur, Some comments on models for Fischer–Tropsch reaction in slurry bubble column reactors, Chem.Engng. Sci. 38 (1983) 441–446.

[9] W.D. Deckwer, Y. Serpemen, M. Ralek, B. Schmidt, Modeling the Fischer–Tropsch synthesis in the slurry phase, Ind. Eng. Chem. Process Des. Dev. 21 (1982) 231–241.

[10] D. Stern, A.T. Bell, H. Heinemann, A theoretical model for the performance of bubble-column reactors used for Fischer–Tropsch synthesis, Chem.Engng. Sci. 40 (1985) 1665–1677.

[11] S.C. Saxena, M. Rosen, D.N. Smith, J.A. Ruether, Mathematical modeling of Fischer–Tropsch slurry bubble column reactors, Chem. Engng. Commun. 40 (1986) 97–151.

[12] P.L. Mills, J.R. Turner, P.A. Ramachandran, M.P. Dudukovic, The Fischer–Tropsch synthesis in slurry bubble column reactors: analysis of reactor performance using the axial dispersion model, in: A. Schumpe, K.D.P. Nigam (Eds.), Three Phase Sparged Reactors, Gordon & Breach, New York, 1996 Chapter 5.

[13] C. Maretto, R. Krishna, Modelling of a bubble column slurry reactor for Fischer–Tropsch synthesis, Catalysis Today 52 (1999) 279–289.

[14] G.P. Van der Laan, A.A.C.M. Beenackers, R. Krishna, Multicomponent reaction engineering model for Fe-catalysed Fischer–Tropsch synthesis in commercial scale bubble column slurry reactors, Chem. Engng. Sci. 54 (1999) 5013–5019.

[15] D.J. Vermeer, R. Krishna, Hydrodynamics and mass transfer in bubble columns operating in the churn-turbulent regime, Ind.Eng.Chem. Process Design & Dev. 20 (1981) 475–482.

[16] R. Krishna, P.M. Wilkinson, L.L. Van Dierendonck, A model for gas holdup in bubble columns incorporating the influence of gas density on flow regime transitions, Chem. Engng Sci. 46 (1991) 2491–2496.

[17] R. Krishna, J. Ellenberger, D.E. Hennephof, Analogous description of gas–solid fluidized beds and bubble columns, Chem. Engng. J. 53 (1993) 89–101.

[18] J. Ellenberger, R. Krishna, A unified approach to the scaleup of gas–solid fluidized and gas–liquid bubble column reactors, Chem. Engng. Sci. 49 (1994) 5391–5411.

[19] R. Krishna, J. Ellenberger, A unifed approach to the scale up of 'fluidized' multiphase reactors, Chem. Engng. Res. Design Trans. I. Chem. E. 73 (1995) 217–221.

[20] J.W.A. De Swart, R. Krishna, Effect of particles concentration on the hydrodynamics of bubble column slurry reactors, Chem. Engng. Res. Design Trans. I. Chem. E. 73 (1995) 308–313.

[21] R. Krishna, J. Ellenberger, S.T. Sie, Reactor development for conversion of natural gas to liquid fuels: a scale up strategy relying on hydrodynamic analogies, Chem. Engng. Sci. 51 (1996) 2041–2050.

[22] J.W.A. De Swart, R.E. van Vliet, R. Krishna, Size, structure and dynamics of 'large' bubbles in a 2-D slurry bubble column, Chem. Engng. Sci. 51 (1996) 4619–4629.

[23] R. Krishna, J. Ellenberger, Gas holdup in bubble column reactors operating in the churn-turbulent flow regime, A.I.Ch.E.J. 42 (1996) 2627–2634.

[24] R. Krishna, J.W.A. de Swart, J. Ellenberger, G.B. Martina, C. Maretto, Gas holdup in slurry bubble columns, A.I.Ch.E.J. 43 (1997) 311–316.

[25] H.M. Letzel, J.C. Schouten, R. Krishna, C.M. van den Bleek, Characterization of regimes and regime transitions in bubble columns by chaos analysis of pressure signals, Chem. Engng. Sci. 52 (1997) 4447–4459.

[26] R. Krishna, J.M. Vanbaten, J. Ellenberger, Scale effects in fluidized multiphase reactors, Powder Technology 100 (1998) 137–146.

[27] R. Krishna, J.M. Vanbaten, M.I. Urseanu, Three-phase Eulerian simulations of bubble column reactors operating in the churn-turbulent flow regime: a scale up strategy, Chem. Engng. Sci. 55 (2000) 3275–3286.

[28] R. Krishna, J.M. Van Baten, M.I. Urseanu, J. Ellenberger, Design and scale-up of the bubble column slurry reactor for Fischer–Tropsch synthesis, Chem. Engng. Sci. 56 (2001) 537–545.

[29] J.M. Van Baten, R. Krishna, Eulerian simulations for determination of the axial dispersion of liquid and gas phases in bubble columns operating in the churn-turbulent regime, Chem. Engng. Sci. 56 (2001) 503–512.

[30] De Swart J.W.A., Scale up of a Fischer–Tropsch slurry reactor, PhD dissertation, University of Amsterdam, The Netherlands, 1996.

[31] M.F. Post, A.C. Van't Hoog, J.K. Minderhout, S.T. Sie, Diffusion limitations in Fischer–Tropsch catalysts, A.I.Ch.E.J. 35 (1989) 1107–1114.

[32] J.J. Van Deemter, Mixing and contacting in gas–solid fluidized beds, Chem. Engng. Sci. 13 (1961) 143–165.[33]Y Kato, A. Nishiwaki, T. Fukuda, S. Tanaka, The behavior of suspended solid particles and liquid in bubble columns, J. Chem. Engng. Japan 5 (1972) 112–117.

[34] W.D. Deckwer, A. Schumpe, Bubble columns-state of the art and current trends, Ind. Engng.Chem. Process Des. Dev. 27 (1987) 405–422.

[35] N. Devanathan, D. Moslemian, M.P. Dudukovic, Flow mapping in bubble columns using CARPT, Chem. Eng. Sci. 45 (1990) 2285–2291.

[36] O. Levenspiel, Chemical Reaction Engineering, Wiley, New York, 1972.

[37] Bukur D.B., Daly J.G., Patel S.A., Hydrodynamics of three-phase slurry Fischer–Tropsch bubble column reactors, US DOE Final Report No. DOE/PC/90012-10, Department of Energy, USA, 1990

[38] S. Peter, M. Weinert, Die diffusionsgeschwindigkeit des wasserstoffs in kohlenwasserstoffen bei hohen drucken, Z. Phys. Chem. 9 (1956) 114–121.

[39] S. Peter, M. Weinert, Uber die Loslichkeit von H_2, CO, CO_2 und Wasserdampf in flussigen Kohlenwasserstoffen, Z. Phys. Chem. 5 (1955) 49–61.
[40] Wilkinson P.M., Physical aspects and scale-up of high presure bubble columns, PhD thesis, Groningen, The Netherlands, 1991.
[41] P.H. Calderbank, M.B Mooyoung, The continuous phase heat and mass-transfer properties of dispersions, Chem. Eng. Sci. 16 (1961) 39–54.
[42] W.E. Schiesser, The Numerical Method of Lines: Integration of Partial Differential Equations, Academic Press, San Diego, 1991.
[43] C.A. Silebi, W.E. Schiesser, Dynamic Modeling of Transport Process Systems, Academic Press, San Diego, 1992.
[44] Hindmarsh A.C., LSODE and LSODI, Two new initial value ordinary differential equation solvers, A.C.M. — Signum Newsletter, 15, (1980), 10-11.
[45] R.W. Field, J.F. Davidson, Axial dispersion in bubble columns, Trans. I. Chem. E. 58 (1980) 228–236.